On the Design of Front-To-Total Anti-roll Moment Distribution Controllers for Enhancing the Cornering Response

Marco Ricco, Matteo Dalboni, Patrick Gruber, Miguel Dhaens, and Aldo Sorniotti

Abstract

In the last three decades a relatively wide literature has discussed the potential vehicle dynamics benefits of the control of the front-to-total anti-roll moment distribution generated by active suspension systems, either based on actuators located within the individual corners or controllable anti-roll bars. However, because of the nonlinearity of the involved phenomena, there is a lack of systematic model based design routines to achieve the reference cornering response in steady-state and transient conditions through active suspension controllers, and for the integration of suspension control with direct yaw moment control. This paper targets such knowledge gap, by introducing design tools for front-to-total anti-roll moment distribution control, based on: i) optimizations using a quasi-static model for the computation of the non-linear feedforward contribution of the controller; ii) a novel linearized vehicle model formulation for linear control design in the frequency domain; and iii) a nonlinear vehicle model formulation to be used as prediction model for nonlinear model predictive control. A set of simulation and experimental results shows the benefits in terms of: a) understeer gradient tunability; b) increased maximum achievable lateral acceleration; c) increased yaw and sideslip damping; and d) energy consumption reduction.

M. Ricco · M. Dalboni · P. Gruber · A. Sorniotti
University of Surrey, Guildford, UK

A. Sorniotti
e-mail: a.sorniotti@surrey.ac.uk

M. Dhaens (✉)
Tenneco Automotive, Sint-Truiden, Belgium
e-mail: mdhaens@driv.com

1   Introduction

Among their many functions, active suspension systems, either based on inde-
pendent actuators at the vehicle corners or controllable anti-roll bars, are usually
adopted to significantly reduce the roll motion caused by the lateral acceleration
in cornering, through the generation of an appropriate anti-roll moment. More-
over, these systems can also regulate the distribution of the anti-roll moment
between the front and rear axles, which is directly related to the lateral load trans-
fer distribution. The lateral load transfers deteriorate the lateral axle force capa-
bility, as the lateral force increment on the laden tire is smaller than the lateral
force decrease on the unladen tire. Hence, when the load transfer is increased, a
larger slip angle is required to generate the same lateral axle force. Therefore, a
front-to-total anti-roll moment distribution controller can vary the slip angle dif-
ference between the axles, i.e., the level of vehicle understeer, see [1, 2].

The general trend toward model based control requires simplified vehicle
models for control design, or internal models for model predictive control. Due
to the important nonlinearity in the effect of the lateral load transfer on vehi-
cle dynamics, it is necessary to formulate mathematical models that, although
approximated, are still able to catch the fundamental implications of load transfer.
In [3]–[7] the authors use the commonly adopted parabolic relationship between
the individual vertical tire load and its cornering stiffness, which brings a quad-
ratic reduction of the axle cornering stiffness with the lateral load transfer, under
the simplifying hypothesis of linear lateral axle force as a function of slip angle,
which is a major limitation. Lakehal-Ayat et al. [8] describe the lateral axle force
through a nonlinear vehicle model including a combination of parabolic cornering
stiffness and simplified Pacejka magic formula.

In [9], while discussing linear vehicle models, Genta notes that "it is impos-
sible to state the effect of anti-roll bars" on the yaw rate, sideslip angle and lat-
eral acceleration gains, "as they introduce a strong nonlinearity...and the very
definition of the gains is based on a complete linearization." Therefore, many
authors use heuristics for the design of anti-roll moment distribution controllers.
For example, on/off rules are proposed in [10]; in [11] the front-to-total anti-roll
moment distribution ratio is proportional to the yaw rate error, with a gain

depending on the lateral acceleration, while a fuzzy proportional integral derivative (PID) controller is adopted in [12]. In [13] Abe states that "as the effect of the lateral load transfer on the lateral/directional dynamics in itself is strongly nonlinear, it is difficult to derive the control law by using the fully analytical method. Therefore, this paper concentrates on computer simulation of vehicle response" for control design. In [14], Cooper et al. explain that "the inverse model could not model the tyre nonlinearities sufficiently while still remaining simple enough…. Due to this, PID control was implemented for roll moment distribution." Similarly, Yan et al. [15] report that "due to the nonlinear properties of four tires and the complicated dynamic information of the whole vehicle system, the distribution coefficient for yaw response characteristics is difficult to be accurately described, which means that the modern design method of control algorithm based on state equation is not applicable." In the integrated chassis controller of [16], the front-to-total anti-roll moment distribution parameter is controlled through an empirical law, using a sideslip based stability index and the yaw rate error, without model based control.

In conclusion, there is a gap in model based design methodologies of front-to-total anti-roll moment distribution controllers, to achieve a-priori defined steady-state and transient cornering responses through linear and/or nonlinear control techniques. This paper discusses the following items on anti-roll moment distribution control, from very recent studies by the authors [17]–[19]:

- A model based design routine of the nonlinear feedforward control contribution.
- A Model for Linear Control System Design
- A simplified model for nonlinear model predictive control design.
- Two examples of performance assessments of the resulting controllers.

2 Effect of Lateral Load Transfer on Lateral Axle Force and Cornering Stiffness

Figure 1 shows an example of variation of the lateral tire force, $F_{t,y}$, as a function of slip angle, α, for different values of vertical tire load, $F_{t,z}$, by using the Pacejka magic formula (version 5.2) [20], for slip ratio and camber angle equal to zero. The lateral tire force gradient decreases with α, and eventually becomes negative for the specific tire. Very importantly, for a fixed value of α, $F_{t,y}$ varies with $F_{t,z}$ in a nonlinear fashion, i.e., the increment of $F_{t,y}$ is less than linearly proportional to the increment of $F_{t,z}$.
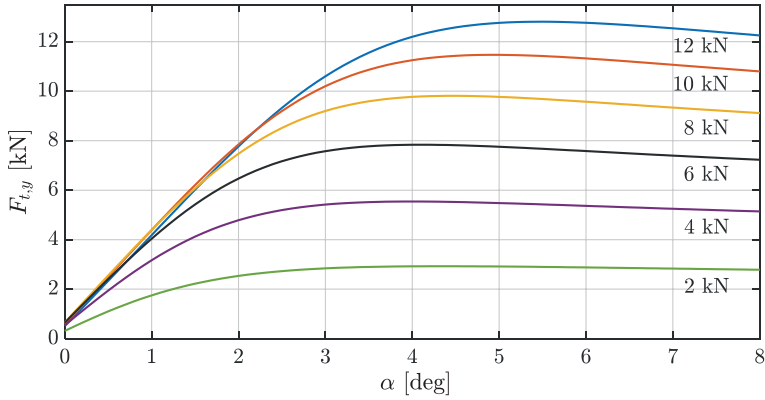
Fig. 1. Lateral tire force as a function of slip angle for vertical tire loads from 2 to 12 kN

For the tires of Fig. 1, Fig. 2 shows the variation of the lateral axle force, F_y, resulting from the sum of the individual lateral tire forces, under the assumption of lateral load transfers ΔF_z, while Fig. 3 reports the variation of the axle cornering stiffness, C, defined as the local gradient of the $F_y(\alpha)$ characteristic. F_y decreases when ΔF_z increases, which is the main effect, while, depending on the slip angle, C can increase or decrease with increasing ΔF_z.

The consequence is that for a given lateral acceleration, an increment of the lateral load transfer on the front axle, with a corresponding decrement on the rear axle, increases understeer, which, vice versa, is reduced by an increase of the rear axle load transfer. Therefore, in quasi-steady-state cornering, active suspension control allows shaping the understeer characteristic and increasing the maximum achievable lateral acceleration, while during transients it can increase yaw and sideslip damping, and thus enhance active safety.
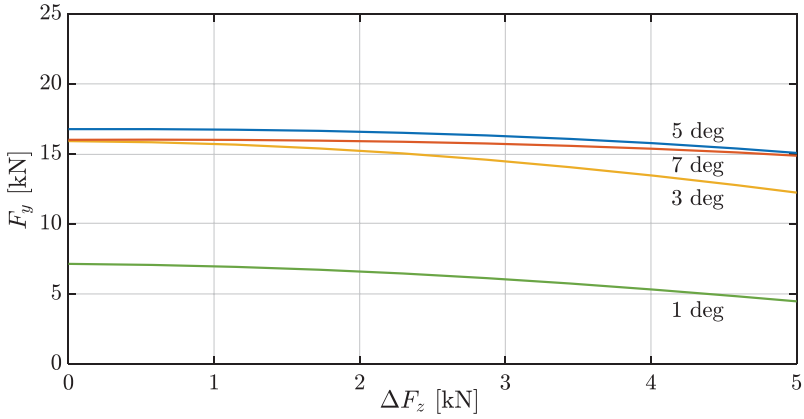
Fig. 2. Lateral axle force as a function of lateral load transfer for slip angles from 1 to 7 deg, with a static axle load of 11.6 kN
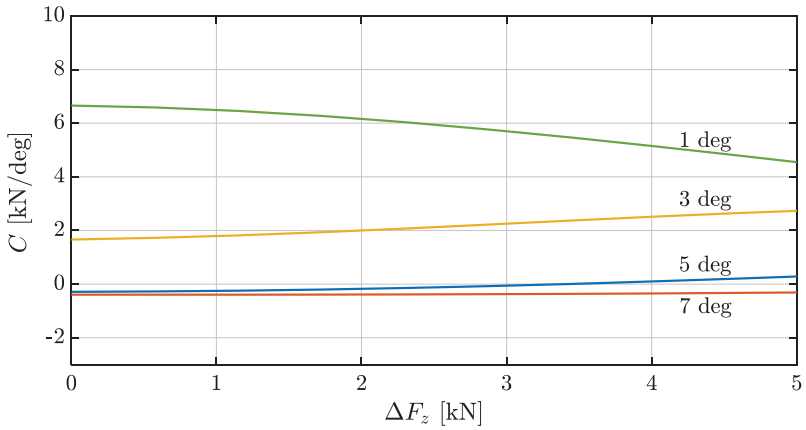

Fig. 3. Axle cornering stiffness as a function of lateral load transfer for slip angles from 1 to 7 deg, with a static axle load of 11.6 kN

3   Model Based Design of the Steady-State Nonlinear Feedforward Contribution

This section discusses a routine for the offline model based design of the map of the nonlinear feedforward contribution of the anti-roll moment distribution, to achieve a reference cornering response in terms of understeer characteristic. The routine consists of the following steps, using a nonlinear quasi-static vehicle model formulation, see its details in [17]:

Step 1: minimization of the absolute value of the dynamic steering angle, $|\delta_{Dyn}|$, which is the cost function J of the optimization using the quasi-static model:

$$\min_{\text{arg}f}(J) = \min_{\text{arg}f}|\delta_{Dyn}| = \min_{\text{arg}f}|\delta - \delta_{Kin}| \tag{1}$$

δ_{Dyn} is the difference between the average steering angle of the front wheels, δ, and the kinematic steering angle, δ_{Kin}. Hence, the optimization outputs the limit understeer characteristic ('Limit' in Fig. 4), i.e., the one that makes the vehicle as close as possible to the neutral steering behavior, together with the corresponding values of f, which is the front-to-total anti-roll moment distribution parameter for the active part of the anti-roll moment:

$$f = \frac{M_{AR,Act,F}}{M_{AR,Act,F} + M_{AR,Act,R}} \tag{2}$$

where $M_{AR,Act,F}$ and $M_{AR,Act,R}$ are the front and rear active anti-roll moments.

Step 2: selection of the reference understeer characteristic, $\delta_{Dyn,Ref}(a_y)$, where a_y is the lateral acceleration. Since the understeer characteristic from Step 1 is usually not suitable for a real-world application as the driver normally prefers some level of understeer to indicate when the cornering limit is approached, in the control design phase $\delta_{Dyn,Ref}(a_y)$ is selected to be intermediate between that of the passive vehicle and the limit one, through a graphical user interface overlapping the different characteristics. $\delta_{Dyn,Ref}(a_y)$ ('Ref.' in Fig. 4) is approximated with a linear function up to the lateral acceleration a_y^*, and a logarithmic function for higher lateral accelerations:

$$\delta_{Dyn,Ref} = \begin{cases} k_{US}a_y; a_y < a_y^* \\ k_{US}a_y^* + [a_y^* - a_{y,Max}]k_{US}\log\left(\frac{a_y - a_{y,Max}}{a_y^* - a_{y,Max}}\right); a_y \geq a_y^* \end{cases} \tag{3}$$

where k_{US} is the understeer gradient in the linear part of the characteristic; and $a_{y,Max}$ is the maximum reference lateral acceleration. k_{US}, a_y^*, and $a_{y,Max}$ are user-defined parameters (examples of values are reported in Fig. 4).

Step 3: recalculation of the reference understeer characteristic from Step 2 in terms of actual steering angle and vehicle speed V, to obtain $\delta_{Ref}(a_y, V)$:

$$\delta_{Ref}(a_y, V) = \delta_{Dyn,Ref}(a_y) + \frac{la_y}{V^2} \tag{4}$$

Step 4: calculation of the reference yaw rate characteristic. $\delta_{Ref}(a_y, V)$ from Step 3 is manipulated and interpolated to obtain the reference lateral acceleration characteristic, $a_{y,Ref}(\delta, V)$. The map of the steady-state reference yaw rate is derived as $r_{Ref}(\delta, V) = a_{y,Ref}(\delta, V)/V$. r_{Ref} is the yaw rate that makes the vehicle follow the reference understeer characteristic.

Step 5: design of the steady-state feedforward front-to-total anti-roll moment distribution ratio, $f_{FFW,SS}$ (Fig. 5). $r_{Ref}(\delta, V)$ from Step 4 is imposed as a further equality constraint in the optimization, which is run without a cost function, as the number of equality constraints is equal to the number of variables. Step 5 can include a cost function in case of presence of further active chassis control systems, e.g., based on direct yaw moment control or rear-wheel-steering.

$f_{FFW,SS}(\delta, V)$, together with $r_{Ref}(\delta, V)$, is stored in look-up tables in the vehicle control unit. Additional variables, such as the longitudinal acceleration or total torque demand, could be used as optimization parameters and map inputs, depending on the specific requirements. In the online implementation, $f_{FFW,SS}(\delta, V)$ is typically filtered through an appropriate transfer function, which outputs f_{FFW}. To prevent undesired system response, a progressive deactivation algorithm of the feedforward contribution is recommended, which imposes f_{Nom}, i.e., the nominal front-to-total distribution of the passive vehicle, in case of significant absolute values of the yaw rate error, or estimated rear axle sideslip angle, $\left|\widehat{\beta}_{RA}\right|$.
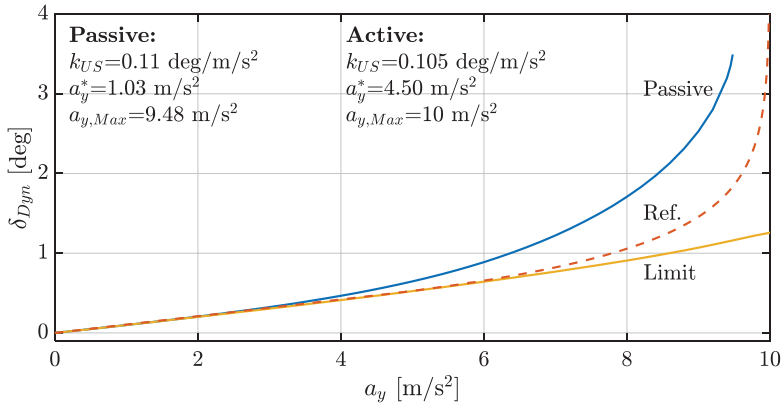
Fig. 4. Examples of understeer characteristic of the passive vehicle ('Passive'), limit understeer characteristic ('Limit'), and reference understeer characteristic of the active vehicle ('Ref.')
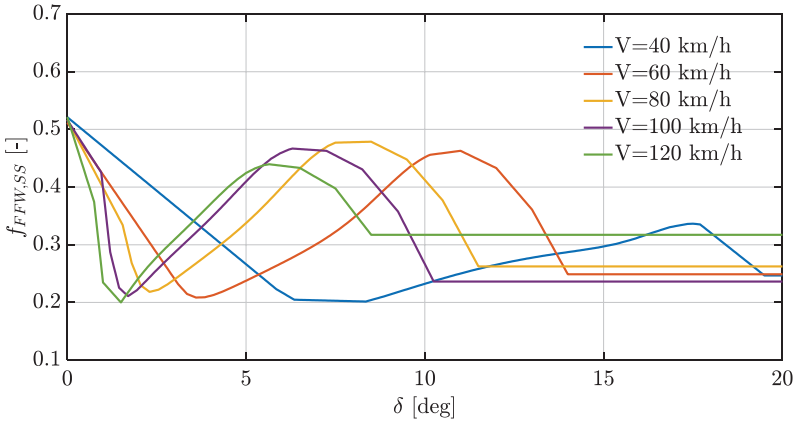

Fig. 5. Example of steady-state feedforward front-to-total anti-roll moment distribution map

4   Model for Linear Control Design

The proposed lateral axle force model expresses the relationship between $F_{y,i}$, α_i and $\Delta F_{z,i}$, around a linearization point defined by $F_{y,i,0}$, $\alpha_{i,0}$ and $\Delta F_{z,i,0}$, corresponding to an axle cornering stiffness $C_{i,0}$ for a given operating condition of the vehicle, where the subscript $i = F, R$ indicates the front or rear axles. For a given $\Delta F_{z,i}$, $F_{y,i}$ is represented as a linear function of α_i:

$$F_{y,i} \approx F_{y,i,lin} + C_i[\alpha_i - \alpha_{i,0}] \tag{5}$$

In accordance to Figs. 2 and 3, $F_{y,i,lin}$ and C_i vary with $\Delta F_{z,i}$, which can be expressed through a first order Taylor series expansion around $\Delta F_{z,i,0}$:

$$
\begin{aligned}
F_{y,i,lin} &\approx F_{y,i,0} + F'_{y,i,0}[\Delta F_{z,i} - \Delta F_{z,i,0}] \\
C_i &\approx C_{i,0} + C'_{i,0}[\Delta F_{z,i} - \Delta F_{z,i,0}]
\end{aligned}
\tag{6}
$$

where $F'_{y,i,0}$ and $C'_{i,0}$ are the gradients of the lateral axle force and axle cornering stiffness with respect to the lateral load transfer, which can be derived from Figs. 2 and 3. By combining (Eq. 5) and (Eq. 6), the complete formulation becomes:

$$F_{y,i} \approx F_{y,i,0} + F'_{y,i,0}[\Delta F_{z,i} - \Delta F_{z,i,0}] + \left\{ C_{i,0} + C'_{i,0}[\Delta F_{z,i} - \Delta F_{z,i,0}] \right\}[\alpha_i - \alpha_{i,0}] \tag{7}$$

The resulting vehicle model has three degrees of freedom, i.e., it is based on the lateral force, roll moment and yaw moment balance equations:

$$
\begin{aligned}
mV[\dot{\beta} + r] &= F_{y,F} + F_{y,R} \\
I_z \dot{r} &= F_{y,F} a_F - F_{y,R} a_R + M_{z,Ext} \\
I_x \ddot{\varphi} = mV[\dot{\beta} + r]h_{roll} &+ mgh_{roll}\varphi - M_{AR,Pass,F} - M_{AR,Pass,R} \\
&- M_{AR,Act,F} - M_{AR,Act,R}
\end{aligned}
\tag{8}
$$

where m is the vehicle mass; r is the yaw rate; $\dot{\beta}$ is the sideslip rate; I_z is the yaw mass moment of inertia; $M_{z,Ext}$ is an external yaw moment, e.g., caused by direct yaw moment control through the friction brakes or multiple electric motors; I_x is the roll mass moment of inertia; φ is the roll angle; h_{roll} is the distance between the center of gravity and roll axis; g is the gravitational acceleration; and $M_{AR,Pass,F}$ and $M_{AR,Pass,R}$ are the front and rear passive anti-roll moment contributions, described by:

$$M_{AR,Pass,F} = K_F\varphi + D_F\dot{\varphi} \tag{9}$$

$$M_{AR,Pass,R} = K_R\varphi + D_R\dot{\varphi}$$

where K_F and K_R are the front and rear axle roll stiffness values, and D_F and D_R are the respective roll damping coefficients.

The active anti-roll moments can be expressed as functions of a_y:

$$M_{AR,Act,F} = kma_yh_{roll}f = kmV\left[\dot{\beta} + r\right]h_{roll}f$$
$$M_{AR,Act,R} = kma_yh_{roll}\left[1-f\right] = kmV\left[\dot{\beta} + r\right]h_{roll}\left[1-f\right] \tag{10}$$

where ma_yh_{roll} is the total roll moment caused by the vehicle's lateral acceleration; and the gain k indicates the level of roll moment compensation of the active suspension system, i.e., $k = 0$ indicates no compensation and $k = 1$ indicates full compensation.

Under the small angle approximation, the front and rear slip angles, α_F and α_R, are:

$$\alpha_F \approx \beta + \frac{a_F}{V}r - \delta$$
$$\alpha_R \approx \beta + \frac{a_R}{V}r \tag{11}$$

The lateral load transfer is calculated from the total anti-roll moment of the axle, $M_{AR,tot,i} = M_{AR,Pass,i} + M_{AR,Act,i}$, see [18].

By combining and re-arranging the previous equations, the model formulation is obtained:

$$\begin{cases} \dot{x} = q(x,u,w) \\ y = h(x,u,w) \end{cases} \tag{12}$$

where q and h are nonlinear functions; and the state, input, disturbance and output vectors, respectively x, u, w and y, are:

$$x = \begin{bmatrix} \beta \\ r \\ \varphi \\ \dot{\varphi} \end{bmatrix}, u = \begin{bmatrix} f \end{bmatrix}, w = \begin{bmatrix} \delta \\ M_{z,Ext} \end{bmatrix}, y = \begin{bmatrix} \beta \\ r \\ \varphi \\ a_y \\ \Delta F_{z,F} \\ \Delta F_{z,R} \end{bmatrix} \tag{13}$$

In (Eq. 13), δ and $M_{z,Ext}$ are considered disturbances if they are not calculated by the controller; however, the input vector can be augmented with additional control inputs, such as the front and rear steering angles and direct yaw moment.

Differently from the conventional single track model formulation, (Eq. 12) is nonlinear, because of the terms related to: a) the suspension control action, f; b) the variation of the lateral axle force with the lateral load transfer, $F'_{y,i,0}$; and c) the variation of the cornering stiffness with the lateral load transfer, $C'_{y,i,0}$. To obtain a linear model, the system variables are expressed with respect to the linearization point:

$$x = x_0 + \Delta x \quad u = u_0 + \Delta u \quad w = w_0 + \Delta w \quad y = y_0 + \Delta y \tag{14}$$

where x_0, u_0, w_0 and y_0 are the vector values at the linearization point; and the symbol Δ indicates a deviation. As $\dot{x}_0 = q(x_0, u_0, w_0)$ and $y_0 = h(x_0, u_0, w_0)$, the linearization of (Eq. 12), which can be derived through appropriate symbolic calculation software, has the following form:

$$\begin{cases} \Delta\dot{x} = A\Delta x + B\Delta u + E\Delta w \\ \Delta y = C\Delta x + D\Delta u + F\Delta w \end{cases} \tag{15}$$

where A, B and E are the state, input and disturbance matrices; and C, D and F are the respective output equation matrices. The formulation in (Eq. 15) can be used for state space control design techniques, or for obtaining the transfer function $\Delta r/\Delta f$, which is the basis for control system design in the frequency domain, see the theory in [21] and the suspension control example in [18].

5 Internal Model for Nonlinear Model Predictive Control

Some of the state-of-the-art chassis control implementations adopt nonlinear model predictive control (NMPC) techniques, which are based on predictions using a nonlinear model of the system. For example, the recent front-to-total anti-roll moment distribution controller in [19] uses a double track model, including the longitudinal, lateral roll and yaw degrees of freedom, as well as wheel rotations. The model considers the effect of the longitudinal and lateral load transfers.

The key aspect of the prediction model is the tire force formulation, based on a simplified version of the Pacejka magic formula, which allows the computation of the longitudinal and lateral tire forces, $F_{t,x,ij}$ and $F_{t,y,ij}$, while considering the effect of the load transfers induced by the active suspension system:

$$F_{t,x,ij} = \frac{s_{x,ij}}{s_{ij}} \mu_{x0,ij} F_{t,z,ij} \tag{16}$$

$$F_{t,y,ij} = \frac{s_{y,ij}}{s_{ij}} \mu_{y0,ij} F_{t,z,j} \tag{17}$$

where the subscript $j = L, R$ indicates the left or right corner. $\mu_{x0,ij}$ and $\mu_{y0,ij}$ are given by:

$$\mu_{x0,ij} = D_x \sin\left(C_x \arctan\left(B_x s_{ij}\right)\right) \tag{18}$$

$$\mu_{y0,ij} = D_{y,ij} \sin\left(C_y \arctan\left(B_y s_{ij}\right)\right) \tag{19}$$

where s_{ij} is the combined theoretical slip:

$$s_{ij} = \sqrt{s_{x,ij}^2 + s_{y,ij}^2} \tag{20}$$

with:

$$s_{x,ij} = \frac{\sigma_{ij}}{1 + \sigma_{ij}} \tag{21}$$

$$s_{y,ij} = -\frac{\tan(\alpha_{ij})}{1 + \sigma_{ij}} \tag{22}$$

where σ_{ij} and α_{ij} are the slip ratio and slip angle. In (Eqs. 18)–(19), C_x and C_y are constant, while $D_{y,ij}$ linearly varies with $F_{t,z,ij}$:

$$D_{y,ij} = d_1 F_{t,z,ij} + d_2 \tag{23}$$

where d_1 and d_2 are constant coefficients, for a given tire-road friction condition. The feature in (Eq. 23) allows modeling the nonlinear relationship between lateral tire force and vertical load, which is of the essence for anti-roll moment distribution control. The complete nonlinear optimal control problem formulation is in [19].

6   Examples of Results

6.1   Case Study 1: Anti-roll Moment Distribution Control Using Nonlinear Feedforward and Linear Feedback Contributions

A front-to-total anti-roll moment distribution controller based on the sum of nonlinear feedforward and linear feedback control contributions, designed through the model based methods in Sects. 3 and 4, was preliminarily assessed on a sport utility vehicle (SUV) demonstrator (Fig. 6). The vehicle is equipped with a hydraulic active suspension system, i.e., the Tenneco Monroe intelligent suspension, ACOCAR. At each vehicle corner, a pump pressurizes the hydraulic circuit of the respective actuator and inputs energy into the system. The pressure level in the hydraulic chambers is modulated through the currents of the base and piston valves of the actuator, which is installed in parallel to an air spring.

Fig. 6. Case study demonstrator vehicle

A centralized skyhook algorithm and roll angle compensation controller, already installed and tested on the SUV, were integrated with the front-to-total anti-roll moment distribution controller, characterized by a Sport mode and a Normal mode, selectable by the user. For ease of implementation, a proportional integral (PI) controller was used for the feedback anti-roll moment distribution contribution controlling the yaw rate error, and tuned in the frequency domain with the model in Sect. 4.

During the experiments, the stability controller based on the actuation of the friction brakes was deactivated, to prevent interferences. In this case the so-called passive mode, used as term of comparison, is the same vehicle demonstrator, including the pre-existing skyhook and roll angle compensation algorithms, but excluding the anti-roll moment distribution controller.

The experimental results of skidpad and step steer tests are reported in Figs. 7 and 8. During the skidpad in Sport mode, the SUV is substantially neutral steering up to $a_y \approx 7$ m/s², after which it understeers, to make the driver perceive that the cornering limit is approached. The maximum lateral acceleration of the active vehicle is 9.50 m/s², which is a > 10% improvement with respect to the 8.55 m/s² of the passive mode. Figure 7 also reports the f contributions (total and feedforward); as expected, the feedforward contribution is responsible for the majority of the control effort during the skidpad. The step steer of Fig. 8, from an initial speed of 110 km/h and with a steering wheel angle amplitude of 90 deg, highlights the yaw rate damping and sideslip limitation capability of the feedback contribution, i.e., the sideslip angle peak is reduced by the controller, while its steady-state value is approximately the same as for the passive mode.
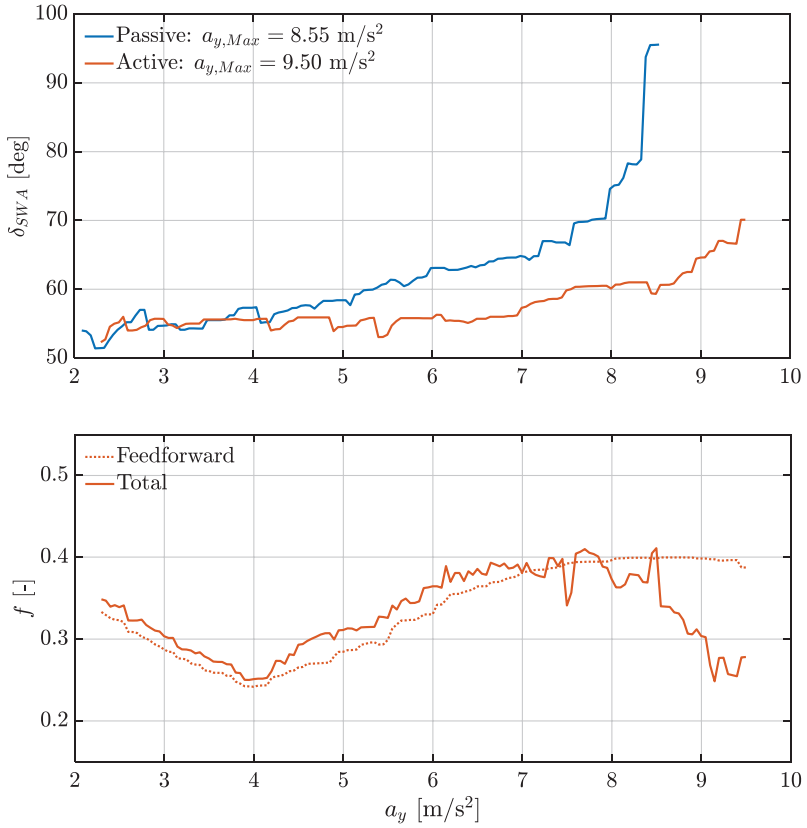
Fig. 7. Experimental skidpad test results in Sport mode: steering wheel angle (δ_{SWA}, top) and front-to-total anti-roll moment distribution parameter (f, bottom) as functions of lateral acceleration (a_y)
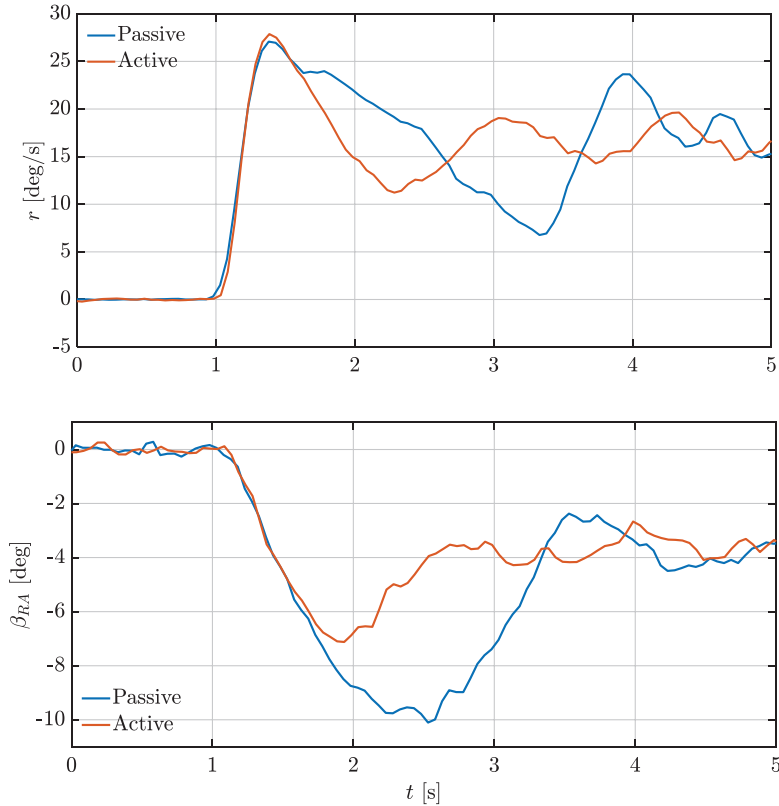
Fig. 8. Experimental step steer results in Normal mode: yaw rate (r, top) and rear axle sideslip angle (β_{RA}, bottom) as functions of time (t)

6.2 Case Study 2: Nonlinear Model Predictive Control for Integrated Torque-Vectoring and Front-To-Total Anti-roll Moment Distribution

The second case study (from [19]) is a nonlinear model predictive control implementation – designed through the model in Sect. 5 – for concurrent front-to-total anti-roll moment distribution control and torque-vectoring (TV) control, i.e., continuously active direct yaw moment control through individual wheel torque distribution. The considered vehicle is the electric SUV of the European project

EVC1000, which is simulated with a high-fidelity and experimentally validated model, and is equipped with in-wheel motors, a brake-by-wire system with independent control of the clamping force of each brake caliper, and active suspension actuators. On top of controlling vehicle dynamics, the NMPC formulation targets the minimization of the relevant power loss contributions, namely those related to the electric powertrains, friction brakes, and longitudinal and lateral tire slip.

The following vehicle control configurations are compared:

a) $f_{pass} + f_{T,pass}$, with active roll angle compensation through active suspension control with fixed front-to-total anti-roll moment distribution ratio $f_{pass} = 0.67$, which was selected to be aligned with the one of the vehicle configuration without active suspension actuators; zero direct yaw moment, i.e., the total wheel torque is the same on the left and right wheels; and front-to-total wheel torque distribution within each vehicle side according to the fixed ratio $f_{T,pass} = 0.5$, which is the natural baseline choice for a four-wheel-drive vehicle.

b) $f_{pass} + f_{T,act}$, with active roll angle compensation with fixed $f_{pass} = 0.67$; zero direct yaw moment; and variable front-to-total wheel torque distribution according to a ratio, $f_{T,act}$, defined in a look-up table function of the torque on the vehicle side and speed, to minimize the electric powertrain power loss.

c) $f_{pass} + TV$ (NMPC) and $f_{pass} + TV$ (PI), including active roll angle compensation with fixed $f_{pass} = 0.67$, and TV control contributions based on the proposed NMPC or a benchmarking PI. In $f_{pass} + TV$ (PI), the front-to-total wheel torque distribution within each vehicle side uses the fixed ratio $f_{T,pass} = 0.5$.

d) $f_{act} + TV$ (NMPC) and $f_{act} + TV$ (PI), including active roll angle compensation with active anti-roll moment distribution and TV, based on NMPC or PI control (the latter designed through the model in Sect. 4).

In summary, all considered arrangements use the active suspension actuators for roll moment compensation; c) includes direct yaw moment control through TV, while d) includes both direct yaw moment control through TV and anti-roll moment distribution control.

A selection of results along a multiple step steer test at constant accelerator pedal position is reported in Fig. 9 and Table 1, which includes the following performance indicators:

- Δr_{RMS}, i.e., the root mean square (RMS) value of the yaw rate error, which evaluates the tracking performance of the controller and overall vehicle agility.

- $|\beta_{Max}|$, i.e., the maximum absolute value of the vehicle body sideslip angle, which is a vehicle stability indicator.
- $\Delta F_{t,z,RMS}^{y}$, i.e., the RMS value of $F_{t,z,FR} + F_{t,z,RR} - F_{t,z,FL} - F_{t,z,RL}$, which assesses the magnitude of the total lateral load transfer, and thus vehicle rollover propensity.
- V_{end}, i.e., the vehicle speed at the end of the test, which assesses the total power loss at the vehicle level, as the maneuver is executed at constant accelerator pedal position.
- $\overline{P}_{loss+bk}$, i.e., the average value of the sum of the powertrain, friction brakes and tire slip power losses.

The NMPC configurations ensure stable yaw rate tracking, with very small overshoots following each steering angle variation, and effectively constrain sideslip angle, with $|\beta_{max}|$ values lower than 2.5 deg. On the contrary, $f_{pass} + f_{T,pass}$ and $f_{pass} + f_{T,act}$ reach $|\beta_{max}|$ values in excess of 14 deg, and experience significant delays with respect to the steering angle profile in returning to the condition of zero yaw rate and sideslip angle at the end of the test. Although the PI controllers provide desirable vehicle response, the NMPC configurations achieve better yaw rate tracking performance than the corresponding PI counterparts, as demonstrated by the Δr_{RMS} values in Table 1, and the yaw rate profiles in Fig. 9.
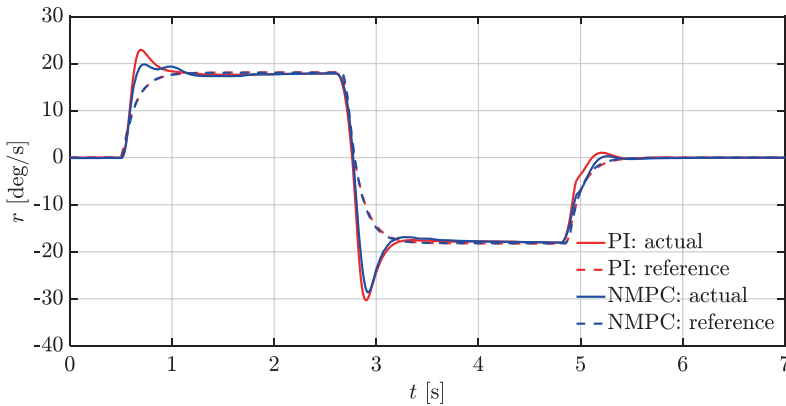

Fig. 9. Simulation results for the multiple step steer test: reference and actual yaw rate profiles for $f_{act} + \text{TV}$ (PI) and $f_{act} + \text{TV}$ (NMPC)

The NMPC and PI configurations bring a reduction of the lateral load transfers during the steering transients, highlighted by the lower values of $\Delta F^y_{t,z,RMS}$. With respect to $f_{act} + \text{TV}$, the increase of $\Delta F^y_{t,z,RMS}$ is negligible for $f_{pass} + \text{TV}$, but it exceeds 20% for $f_{pass} + f_{T,pass}$ and $f_{pass} + f_{T,act}$. After the second steering wheel stroke and the sign inversion of the steering angle, both the front and rear internal wheels lift from the ground in $f_{pass} + f_{T,pass}$ and $f_{pass} + f_{T,act}$, posing a rollover risk, whilst in the NMPC and PI configurations wheel lift only occurs on the front inner corners for more limited time. The NMPC set-ups show very major power loss reductions in transient conditions, with $\overline{P}_{loss+bk}$ values below 53 kW, with respect to the ~96 kW of $f_{pass} + f_{T,pass}$ and $f_{pass} + f_{T,act}$. This difference is mainly caused by the reduction of the lateral tire slip power losses, and is confirmed by the values of V_{end}, ranging from 92.1 km/h for $f_{pass} + f_{T,act}$, to ~115 km/h for the controlled configurations. In terms of power losses, the NMPC solution with active front-to-total anti-roll moment distribution outperforms the one based on TV only, with >12% $\overline{P}_{loss+bk}$ reduction. Significant advantages in terms of energy efficiency are provided by the NMPC set-ups with respect to the corresponding PI alternatives, with 16% and 6% $\overline{P}_{loss+bk}$ reductions for the $f_{pass} + \text{TV}$ and $f_{act} + \text{TV}$ configurations.

Table 1. Performance indicators for the considered vehicle configurations during the multiple step steer test

	Δr_{RMS} [deg/s]	$|\beta_{Max}|$ [deg]	$\Delta F^y_{t,z,RMS}$ [kN]	V_{end} [km/h]	$\overline{P}_{loss+bk}$ [kW]
$f_{pass} + f_{T,pass}$	–	14.66	21.83	92.2	96.13
$f_{pass} + f_{T,act}$	–	14.74	21.84	92.1	96.59
$f_{pass} + \text{TV(NMPC)}$	2.68	2.49	16.52	115.6	52.87
$f_{act} + \text{TV(NMPC)}$	2.66	2.37	16.54	115.1	46.31
$f_{pass} + \text{TV(PI)}$	3.62	2.58	16.38	115.4	62.60
$f_{act} + \text{TV(PI)}$	3.39	2.43	16.87	114.7	49.11

7 Conclusion

The paper outlined three model based design tools for front-to-total anti-roll moment distribution controllers, namely: i) a routine for generating steady-state nonlinear feedforward contribution maps to achieve a reference understeer characteristic; ii) a linearized model for control system design in the frequency

domain; and iii) a simplified nonlinear vehicle model, suitable as prediction model for nonlinear model predictive control implementations. i)-iii) can be used also for the design of integrated controllers, including additional actuators with respect to the active suspension system. Two case study applications highlighted the effectiveness of the methods in i)-iii), through a set of simulation and experimental results in steady-state and transient cornering conditions.

References

1. Danesin D, Krief P, Sorniotti A, Velardocchia M (2003) "Active roll control to increase handling and comfort," SAE Technical Paper 2003–01–0962
2. Clover C, Bernard J (1993) "The Influence of Lateral Load Transfer Distribution on Directional Response," SAE Technical Paper 930763
3. Ren S, Li Z, Yao J, Taheri S (2016) "Improving lateral stability by distributing roll moment via semi-active suspension," FISITA World Automotive Congress
4. Williams DE, Haddad WM (1995) Nonlinear control of roll moment distribution to influence vehicle yaw characteristics. IEEE Trans. on Control Syst Technol 3(1):110–116
5. Wang J, Wilson DA, Xu W, Crolla DA (2005) "Active suspension control to improve vehicle ride and steady-state handling," IEEE Conference on Decision and Control
6. Chu TW, Jones RP (2008) Analysis and simulation of nonlinear handling characteristics of automotive vehicles with focus on lateral load transfer. Veh Syst Dyn 46(1):17–31
7. Bodie MO, Hac A (2000) "Closed loop yaw control of vehicles using magneto-rheological dampers,"AE Technical Paper 2000–01–0107
8. Lakehal-Ayat M, Diop S, Fenaux E (2002) "An improved active suspension yaw rate control," American Control Conference
9. Genta G (1997) "Motor vehicle dynamics: modeling and simulation," World Scientific, 1st ed
10. Xu Y, Ahmadian M (2013) Improving the capacity of tire normal force via variable stiffness and damping suspension system. J. of Terramechanics 50(2):122–132
11. Gerhard J, Laiou MC, Monnigmann M, Marquardt W (2005) Robust yaw control design with active differential and active roll control systems. IFAC Proceedings 38(1):73–78
12. Xinpeng T, Xiaocheng D (2007) "Simulation and study of active roll control for SUV based on fuzzy PID," SAE Technical Paper 2007–01–3570
13. Abe M (1994) "A study on effects of roll moment distribution control in active suspension on improvement of limit performance of vehicle handling," Int. J. of Vehicle Design 15(3/4/5):326–336

14. Cooper N, Crolla D, Levesley M (2005) "Integration of active suspension and active driveline to ensure stability while improving vehicle dynamics," SAE Technical Paper 2005–01–0414

15. Yan M, Pi D, Li Y, Wang H, Wang E (2018) "The design of anti-roll moment distribution for dual-channel active stabilizer bar system," Chinese Control and Decision Conference

16. Termousa H, Shraima H, Taljb R, Francisa C, Charara A (2019) Coordinated control strategies for active steering, differential braking and active suspension for vehicle stability, handling and safety improvement. Veh Syst Dyn 57(10):1494–1529

17. Ricco M, Zanchetta M, Cardolini Rizzo G, Tavernini D, Sorniotti A, Chatzikomis C, Velardocchia M, Geraerts M, Dhaens M (2019) "On the design of yaw rate control via variable front-to-total anti-roll moment distribution," IEEE Trans. on Vehicular Technology 69(2):1388–1403

18. Ricco M, Percolla A, Cardolini Rizzo G, Zanchetta M, Tavernini D, Dhaens M, Geraerts M, Vigliani A,Tota A, Sorniotti A (2020) "On the model-based design of front-to-total anti-roll moment distribution controllers for yaw rate tracking," Vehicle System Dynamics, pp. 1–28

19. Dalboni M, D. Tavernini D, Montanaro U, Soldati A, Concari C, Dhaens M, Sorniotti A 2021 (in press) "Nonlinear Model Predictive Control for Integrated Energy-Efficient Torque-Vectoring and Anti-Roll Moment Distribution," IEEE/ASME Trans. on Mechatronics

20. Pacejka HB (2012) "Tire and vehicle dynamics," 3rd ed., Butterworth-Heinemann

21. Skogestad S, Postlethwaite I (2007) "Multivariable feedback control: analysis and design," 2nd ed., Wiley